

Quality Control and Calibration of the Dual-Polarization Radar at Kwajalein, RMI

DAVID A. MARKS AND DAVID B. WOLFF

Laboratory for Atmospheres, NASA Goddard Space Flight Center, Greenbelt, and Science Systems and Applications, Inc., Lanham, Maryland

LAWRENCE D. CAREY

Earth System Science Center, The University of Alabama in Huntsville, Huntsville, Alabama

ALI TOKAY

Laboratory for Atmospheres, NASA Goddard Space Flight Center, Greenbelt, and Joint Center for Earth Systems Technology, University of Maryland, Baltimore County, Baltimore, Maryland

(Manuscript received 24 February 2010, in final form 14 September 2010)

ABSTRACT

The dual-polarization weather radar on the Kwajalein Atoll in the Republic of the Marshall Islands (KPOL) is one of the only full-time (24/7) operational S-band dual-polarimetric (DP) radars in the tropics. Through the use of KPOL DP and disdrometer measurements from Kwajalein, quality control (QC) and reflectivity calibration techniques were developed and adapted for use. Data studies in light rain show that KPOL DP measurements are of sufficient quality for these applications. While the methodology for the development of such applications is well documented, the tuning of specific algorithms to the particular regime and observed raindrop size distributions requires a comprehensive testing and adjustment period. Presented are algorithm descriptions and results from five case studies in which QC and absolute reflectivity calibration were performed and assessed. Also described is a unique approach for calibrating the differential reflectivity field when vertically pointing observations are not available. Results show the following: 1) DP-based QC provides superior results compared to the legacy Tropical Rainfall Measuring Mission (TRMM) QC algorithm (based on height and reflectivity thresholds), and 2) absolute reflectivity calibration can be performed using observations of light rain via a published differential phase-based integration technique; results are within ± 1 dB compared to independent measurements. Future extension of these algorithms to upgraded Weather Surveillance Radar-1988 Doppler (WSR-88D) polarization diverse radars will benefit National Aeronautics and Space Administration's (NASA's) Precipitation Measurement Missions (PMM) validation programs.

1. Introduction and KPOL site description

Dual-polarimetric (DP) ground-based weather radars are well recognized as vital instruments for applications in hydrology, precipitation microphysics, and hydrometeor identification (Ryzhkov and Zrnica 1998a; Vivekanandan et al. 1999; Straka et al. 2000; Gorgucci et al. 2001; Wang and Carey 2005, among others). Supporting the U.S. Army, and the National Aeronautics and Space Administration's (NASA's) Tropical Rainfall Measuring Mission (TRMM) and Global Precipitation Measurement (GPM)

ground validation (GV) operations at Kwajalein, Republic of the Marshall Islands (Fig. 1), an S-band DP radar (KPOL) operates on a continual basis, providing unique opportunities for algorithm development (Schumacher and Houze 2000; Houze et al. 2004; Wolff et al. 2005; Wang and Wolff 2009; Morris and Schwaller 2009).

A goal of the GPM GV program is to improve the accuracy of rainfall retrievals by developing and improving physically based radiometer algorithms for application over land and ocean. This approach requires insight into the properties of ice microphysics, parameters of local and regional drop size distributions (DSDs), and delineation between water phases. Through careful observation, DP radars can provide a means to cross-validate parameterized microphysical properties in

Corresponding author address: David A. Marks, Code 613.1, SSAI, NASA/GSFC, Greenbelt, MD 20771.
E-mail: david.a.marks@nasa.gov

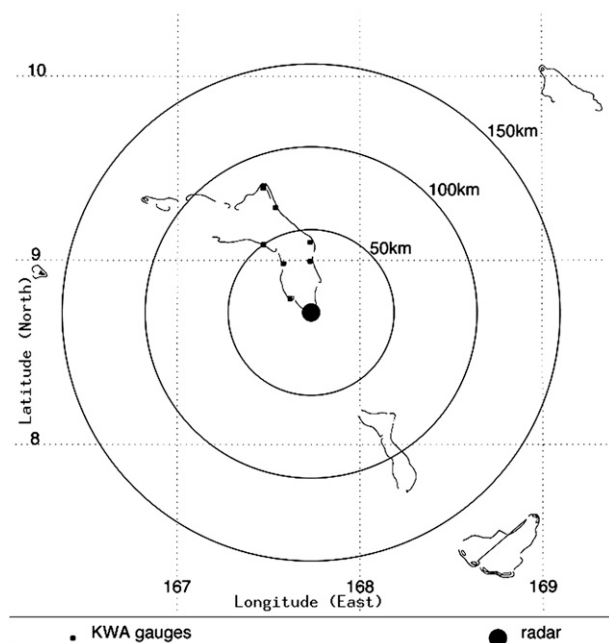


FIG. 1. The location of Kwajalein Atoll (from Wolff et al. 2005). The KPOL S-band radar is located on Kwajalein Atoll at the center of the image (8.7°N, 167.7°E). Rain gauge locations from the KWA network are shown (black squares).

GPM radiometer retrieval algorithms (Kummerow and Petersen 2006; Chandrasekar et al. 2008).

Kwajalein is an oceanic site, and the DP algorithms for quality control (QC), self-consistency calibration, hydrometeor identification, and rain-rate estimation provide an opportunity for the validation of microphysical properties in ocean-based radiometer retrievals from storm to climate scale. KPOL calibration is verified by two independent methods: DP self-consistency (adapted from Ryzhkov et al. 2005) and relative calibration adjustment (RCA; from Silberstein et al. 2008). As discussed in section 3, there is good agreement between the methods.

It is envisioned that DP algorithms (and possibly RCA) can be extended to Weather Surveillance Radar-1988 Doppler (WSR-88D) radar sites for GPM-related and other applied research applications. The TRMM GPM GV programs require continued verification of WSR-88D calibration and QCed data for applied research. The corrected and calibrated DP data will be of value for NASA's Precipitation Measurement Missions (PMM) GV programs by providing observations from numerous meteorological regimes. Deployment of DP diverse WSR-88D radars is scheduled to begin in October 2010 (Istok et al. 2009), so it is relevant that preparations for the upgraded radars are considered.

This manuscript discusses the development and adaptation of DP QC and self-consistency calibration algorithms

with the KPOL radar for the purpose of exploring DP-based validation capabilities. Section 2 describes the overall quality of the KPOL data as compared to established DP research radars, and details the physically based QC techniques applied to the low-level sweeps. The DP QC algorithm is tuned and applied to the lowest two elevation angles to ensure that the data are below the melting level. Section 3 provides a method for the calibration of differential reflectivity and the application of self-consistency reflectivity calibration using properties of the rainfall medium. The predominance of light rain at Kwajalein is ideal for the self-consistency calibration technique of Ryzhkov et al. (2005), wherein calculated and estimated phase data are compared to determine absolute reflectivity bias. Finally, methods and results are summarized in section 4, and considerations for extending the DP algorithms to WSR-88D radars for NASA's PMM GV programs are discussed.

2. KPOL quality control

a. Data quality

KPOL was upgraded to DP capability in early 1998. Basic KPOL characteristics, routinely observed parameters, and scanning strategies are shown in Tables 1 and 2. Because of a litany of engineering and mechanical issues with KPOL (Houze et al. 2004; Marks et al. 2009), DP data were not reliable until 2006. To determine the basic quality of KPOL DP data, empirical comparisons were made with two established DP research radars. The National Center for Atmospheric Research (NCAR) S-band dual-polarization Doppler radar (S-Pol; Lutz et al. 1995) and the Colorado State University–University of Chicago–Illinois State Water Survey (CSU–CHILL) S-band polarimetric radar [see Brunkow et al. (2000); both of which have klystron transmitters] were used as comparison benchmarks to evaluate relative KPOL performance. This was accomplished through analysis of DP measurements in very light rain (defined as $20 \text{ dBZ} \leq Z_H \leq 28 \text{ dBZ}$, where Z_H is the horizontal reflectivity component). In this context, drops are essentially spherical with little or no variability in shape, canting angle, or scattering properties within a radar resolution volume (Doviak and Zrnica 1993). Therefore, DP measurements from this medium are used as indicators of data quality.

In polarimetric radar applications, the copolar correlation coefficient (ρ_{HV}) is a measure of the correlation between horizontally and vertically polarized weather signals. It is primarily affected by the variability in the ratio of the vertical-to-horizontal size of hydrometeors in the resolution volume. Theoretical values of ρ_{HV} larger than 0.99 are indicated by Sachidananda and Zrnica (1985)

TABLE 1. KPOL basic characteristics, moments recorded, and field descriptions.

Transmitter	Magnetron
Processor	SIGMET RVP8/RCP8 combination
Frequency	2.8 GHz
Wavelength	10.71 cm
Beamwidth	1.1° (horizontal and vertical)
Operation mode	Linear, horizontal, and vertical simultaneous dual transmit and receive (STAR)
Moments recorded	
Z_H	Reflectivity, horizontal component
V_r	Radial velocity
σ_v	Spectrum width
Z_{DR}	Differential reflectivity
Φ_{DP}	Total differential phase
K_{DP}	Specific differential phase (processor computed)
$\rho_{HV}(0)$	Copolar cross correlation at zero lag
Field-variable descriptions (with associated units) for KPOL data	
ZT (dBZ)	Raw reflectivity, horizontal component
DZ (dBZ)	SIGMET ground clutter-corrected reflectivity, horizontal component
CZ* (dBZ)	Quality-controlled reflectivity, horizontal component
VR ($m s^{-1}$)	Radial velocity
DR (dB)	Differential reflectivity
PH (°)	Total differential phase
KD ($^{\circ} km^{-1}$)	Specific differential phase
RH (no units)	Copolar cross correlation
SW ($m s^{-1}$)	Spectrum width
SQ (no units)	Signal quality index

* The CZ field is added by the NASA TRMM Satellite Validation Office and contains the reflectivity data that have been corrected for nonprecipitation echo and absolute calibration error.

because of the small shape effects in rain, but theory does not account for possible decreases resulting from side-lobes and receiver noise. Measurements in rain indicate an average ρ_{HV} of 0.98 (Doviak and Zrnicek 1993) with a standard deviation of 0.01. Therefore, the significant deviation (>0.01) of ρ_{HV} below 0.98 in light rain is a likely indicator of general radar system issues.

Other values of polarimetric measurements in light rain (Doviak and Zrnicek 1993, their Table 8.1) include the

analysis of both specific differential phase (K_{DP}) and differential reflectivity (Z_{DR}), where median K_{DP} measurements should be approximately $0^{\circ} km^{-1}$, and average deviation of Z_{DR} from its mean value [Eq. (1)] should be approximately 0 dB, that is,

$$\sum_{i=1}^N [Z_{DR}(i) - \overline{Z_{DR}}] / N \approx 0 \text{ dB}, \quad (1)$$

where N is the number of Z_{DR} gates within the light rain dataset. In addition, the average absolute deviation (AAD) of Z_{DR} from its mean [Eq. (2)] provides an error measurement in Z_{DR} that is analogous to the root-mean-square (rms) error (where N is the Z_{DR} sample size),

$$AAD[Z_{DR}] = \sum_{i=1}^N ||Z_{DR}(i) - \overline{Z_{DR}}|| / N. \quad (2)$$

DP observations in light rain were compared from the three S-band radars: CSU-CHILL, S-Pol, and KPOL. Only one volume from CSU-CHILL and S-Pol was available for comparison. Table 3 shows the median ρ_{HV} and K_{DP} measurements (with their standard deviation), the average deviation of Z_{DR} , and the average absolute deviation of Z_{DR} [Eqs. (1) and (2)] for specific light rain events from the three radars under typical operating conditions. The statistical sample size from each radar was similar (~ 5100 gates) and was obtained from a sector with uniform light rain. These KPOL measurements appear comparable to those from CSU-CHILL and S-Pol, and are in agreement with the previous discussion for expected observations in light rain.

To determine if K_{DP} data are of sufficient quality for numerous applications (QC, self-consistency calibration, rain-rate estimation, and hydrometeor identification), the standard deviation of total differential phase $\sigma(\Phi_{DP})$ in light rain was examined. As discussed in the literature, a reasonable range for $\sigma(\Phi_{DP})$ should be approximately 2° – 3° or lower for K_{DP} -based applications (for review, e.g., see Doviak and Zrnicek 1993; Bringi and Chandrasekar 2001). The standard deviation was computed at each

TABLE 2. Task configuration of the KPOL radar. Columns are task name, radar polarization, elevation angles ($^{\circ}$), and pulse repetition frequency (PRF). Ground validation volume scans initially alternated between A and B (GVVOL_A and GVVOL_B), with one surveillance scan (Surv_TRMM) between volume scan sets. There were 10 volume scans per hour (five A scans and five B scans). The alternating scanning was replaced with a single 17-elevation volume scan (GVVOL) with six volume scans per hour in October 2008.

Task	Polarization	Elevation angles ($^{\circ}$)	PRF
GVVOL_A	Dual	0.4, 1.4, 2.3, 4.2, 6.1, 8.0, 9.9, 11.8, 14.0, 16.6, 19.6, 23.2	960
GVVOL_B	Dual	0.4, 1.4, 3.3, 5.2, 7.1, 9.0, 10.9, 12.9, 15.2, 18.0, 21.3, 25.3	960
Surv_TRMM	Horizontal	0.4	396
Volume scan strategy beginning October 2008 (alternating volumes A and B replaced)			
GVVOL	Dual	0.4, 1.5, 2.6, 3.7, 4.8, 5.9, 7.0, 8.1, 9.2, 10.3, 11.6, 13.2, 15.2, 17.7, 20.8, 24.6, 29.2, 34.7	960

TABLE 3. Empirical investigation of relative DP radar performance in light rain from the CSU–CHILL, S-Pol, and KPOL radars. Shown are the median values for Z_H , ρ_{HV} , and K_{DP} (with standard deviation in parenthesis), the average deviation of Z_{DR} from its mean value [Eq. (1)], and the average absolute deviation of Z_{DR} [AAD Z_{DR} (Eq. 2)] representing error measurement of the Z_{DR} field. The median standard deviation of the measured differential phase $\sigma(\Phi_{DP})$ (with associated dispersion) provides an indication of phase data quality for use in DP applications. The higher value for KPOL $\sigma(\Phi_{DP})$ is within the acceptable boundaries for DP applications. Considering similar statistical sample sizes (No. of gates), measurements from KPOL in light rain are comparable to those from established by CSU–CHILL and S-Pol polarimetric radars.

Radar name	Time/date (UTC)	No. of gates	Med Z_H (dBZ)	Med ρ_{HV}	Med K_{DP} ($^{\circ} \text{ km}^{-1}$)	$Z_{DR} - \overline{Z_{DR}}$ (dB)	AAD Z_{DR} (dB)	Med $\sigma(\Phi_{DP})$ ($^{\circ}$)
CSU–CHILL	0249 UTC 2 Aug 2010	6675	25.5	0.98(0.01)	0.0(0.0)	0.0	0.2	1.2(0.3)
S-Pol	2139 UTC 26 Jan 1999	5022	22.0	0.99(0.01)	0.0(0.2)	0.0	0.2	1.3(0.8)
KPOL	0600 UTC 3 Aug 2007	5100	22.5	0.99(0.01)	0.0(0.1)	0.0	0.3	2.5(0.6)

range gate from a running, centered 25-gate sample in the radial direction (21-gate sample from CSU–CHILL and S-Pol). This corresponds with 0.2-km gate spacing and the SIGMET RVP8 processor K_{DP} length scale of 5 km. Again, with a similar sample size, the KPOL observations are in good agreement with the other radars (Table 3) and show $\sigma(\Phi_{DP}) \approx 2.5^{\circ}$ with a dispersion of 0.6° . The relatively higher value for KPOL $\sigma(\Phi_{DP})$ (compared to CSU–CHILL and S-Pol) is within acceptable boundaries for the development of K_{DP} -based applications. Statistics from 12 KPOL light rain events (with sample sizes of about 5000 gates each) were analyzed and show similar results for all measurements (not shown). The $\sigma(\Phi_{DP})$ values from the 12 cases ranged from 1.8° to 2.9° (average of 2.4°), with dispersions ranging from 0.5° to 1.0° (with an average of 0.6°). The values are dependent upon the case and dataset analyzed. Collectively, these analyses show that KPOL DP measurements are comparable to the CSU–CHILL and S-Pol radars and are of sufficient quality for algorithm development.

An additional analysis of K_{DP} accuracy for self-consistency calibration is also performed. As discussed in section 3b(1), the self-consistency calibration technique compares processor (or user)-determined K_{DP} with theoretical estimates of K_{DP} (as determined by a consistency relationship). Integrating K_{DP} over a large space–time domain substantially reduces the inherent noisiness of point K_{DP} measurements, thereby allowing lighter rains with relatively low K_{DP} to be acceptable for self-consistency calibration of Z_H . Following Ryzhkov et al. (2005), to obtain a consistency-based reflectivity bias (Z_{BIAS}) within 1 dB, the area–time integral of measured K_{DP} should be estimated within 20% accuracy. The K_{DP} measurements and their standard deviation were analyzed from five KPOL rain cases (Table 4). These are the same cases studied for QC and self-consistency calibration and are discussed in detail in later sections. To determine the accuracy or standard deviation of K_{DP} , we used the expression from Balakrishnan and Zrnich (1989) and Carey et al. (2000),

$$\sigma(K_{DP}) = \frac{\sqrt{3}\sigma(\Phi_{DP})}{N^{1.5}\Delta_r}, \quad (3)$$

where $\sigma(\Phi_{DP})$ is the standard deviation of the total differential phase, N is the number of range gates used in K_{DP} calculations, and Δ_r is the range gate spacing. The length scale for KPOL K_{DP} calculations is 5 km and the gate spacing is 0.2 km; therefore, a 25-gate filter is used for each K_{DP} calculation.

To avoid adverse effects from nonuniform beam filling, data were selected within specified range and azimuth boundaries containing continuous echo. Nonuniform beam filling may cause perturbations in Φ_{DP} (Ryzhkov and Zrnich 1998c; Gosset 2004), subsequently resulting in spuriously large K_{DP} (of both signs) in regions of strongly varying precipitation gradients (Ryzhkov 2007). For the five case studies, $\sigma(\Phi_{DP})$ was calculated over 25 gate blocks from all of the volume scans. The lowest $\sigma(\Phi_{DP})$ observed was 2.40° from the 19 December 2006 case, and the highest was 3.42° from the 11 August 2007 case. Inserting the lowest and highest $\sigma(\Phi_{DP})$ values in (3), the resulting range of $\sigma(K_{DP})$ in the data is from $0.17^{\circ} \text{ km}^{-1}$ to $0.24^{\circ} \text{ km}^{-1}$.

As part of the calibration approach, K_{DP} observations are averaged within each reflectivity interval, and there is an associated reduction in $\sigma(K_{DP})$ relative to the number of statistically independent samples. The total number of K_{DP} samples within each reflectivity interval divided by 25 (the block averaging window) provides the number of statistically independent K_{DP} samples. As explained in

TABLE 4. Five KPOL case studies and time periods selected for analysis of K_{DP} , and applications of quality control and self-consistency calibration.

Case	Time (UTC)
19 Dec 2006	0544–0637
3 Aug 2007	0200–0453
11 Aug 2007	0325–0439
19 Sep 2007	1542–1729
23 Nov 2007	1603–1730

TABLE 5. Reflectivity interval statistics to determine K_{DP} data validity from the 19 Dec 2006 case study. Shown are reflectivity interval, average K_{DP} within the interval, number of independent K_{DP} samples, reduction factor (rounded down) in K_{DP} standard error resulting from averaging, maximum allowed standard deviation of K_{DP} , and the standard deviation range of K_{DP} within the interval.

dBZ bin	K_{DP} avg ($^{\circ} \text{ km}^{-1}$)	No. independent K_{DP} samples	Reduction factor	Max allowed $\sigma(K_{DP})$ ($^{\circ} \text{ km}^{-1}$)	Observed data range $\sigma(K_{DP})$ ($^{\circ} \text{ km}^{-1}$)
30	0.053	1741	41	0.011	0.004–0.006
31	0.059	1833	42	0.012	0.004–0.006
32	0.066	1915	43	0.013	0.004–0.005
33	0.076	1957	44	0.015	0.004–0.005
34	0.088	1906	43	0.018	0.004–0.005
35	0.102	1790	42	0.020	0.004–0.006
36	0.120	1615	40	0.024	0.004–0.006
37	0.141	1402	37	0.028	0.005–0.006
38	0.170	1158	34	0.034	0.005–0.007
39	0.210	945	30	0.042	0.006–0.008
40	0.260	763	27	0.052	0.006–0.009
41	0.321	616	24	0.064	0.007–0.010
42	0.391	501	22	0.078	0.008–0.011
43	0.457	402	20	0.091	0.008–0.012
44	0.543	309	17	0.109	0.010–0.014
45	0.626	236	15	0.125	0.011–0.016
46	0.708	176	14	0.142	0.013–0.018
47	0.822	127	12	0.164	0.015–0.021
48	0.913	79	10	0.183	0.019–0.027

Ryzhkov et al. (2005), the reduction factor in $\sigma(K_{DP})$ resulting from the averaging is defined as the square root of the number of independent samples. The reduction factor is then applied to the $\sigma(K_{DP})$ high and low values to determine the $\sigma(K_{DP})$ range in each reflectivity interval. The resulting range of $\sigma(K_{DP})$ is then compared to the maximum allowed $\sigma(K_{DP})$ to assess data validity.

This statistical technique was applied to each reflectivity interval from Z_{\min} (30 dBZ) to Z_{\max} (48 dBZ) for all of the case studies. The results from the 19 December 2006 case are shown in Table 5 and are similar to the results from all five cases. For each reflectivity interval, Table 5 shows the average K_{DP} , the number of independent K_{DP} samples, the reduction factor in $\sigma(K_{DP})$ (rounded down), the maximum allowed $\sigma(K_{DP})$, and the observed $\sigma(K_{DP})$ (after reduction from averaging). To clarify using the 30-dBZ interval in Table 5 as an example, the average K_{DP} is $0.053^{\circ} \text{ km}^{-1}$. There were 43 526 total K_{DP} samples, so the number of independent samples is 1741 ($43\ 526/25$), resulting in an approximate factor of 41 ($1741^{0.5}$) reduction in $\sigma(K_{DP})$. The range for $\sigma(K_{DP})$ is from $0.004^{\circ} \text{ km}^{-1}$ ($0.17/41$) to $0.006^{\circ} \text{ km}^{-1}$ ($0.24/41$), which is well within the maximum allowed $\sigma(K_{DP})$ of $0.011^{\circ} \text{ km}^{-1}$ (20% of the average K_{DP}). In this reflectivity interval, and in all of the intervals from all of the cases, it is shown that the observed range of $\sigma(K_{DP})$ is below the maximum allowed $\sigma(K_{DP})$. Because of extensive averaging, the K_{DP} data are valid for use in the presented self-consistency calibration method (section

3b). Now that overall quality appears acceptable for application development, data QC is considered.

b. QC techniques

KPOL data are frequently contaminated by ground and sea clutter, multiple-trip echo, and considerable noise. QC algorithms based on DP measurements have shown notable success in objective identification of these and other nonprecipitation features (Ryzhkov and Zrnich 1998b; Zrnich and Ryzhkov 1999; Cifelli et al. 2002). Five KPOL case studies with widespread rainfall from 2006 to 2007 were selected to develop an operational QC algorithm for the detection and removal of nonprecipitation echo. A monthly study from July 2008 was also performed to check the DP QC algorithm in various other conditions, such as from isolated to scattered convection and light showers to periods with only nonprecipitation echo present. Because the primary focus was the detection and removal of nonprecipitation echo during rain events, the discussion concentrates on results from the five individual case studies. In the following discussion, refer to Table 1 for the description of moments and field labels.

The multiple steps of the QC algorithm for the lowest two elevation angles are displayed in flowchart form in Fig. 2. For a primary application of quantitative rainfall estimation, the QC steps are applied below the observed radar bright band and site-specific melting level of approximately 4–5 km (Schumacher and Houze 2000). In

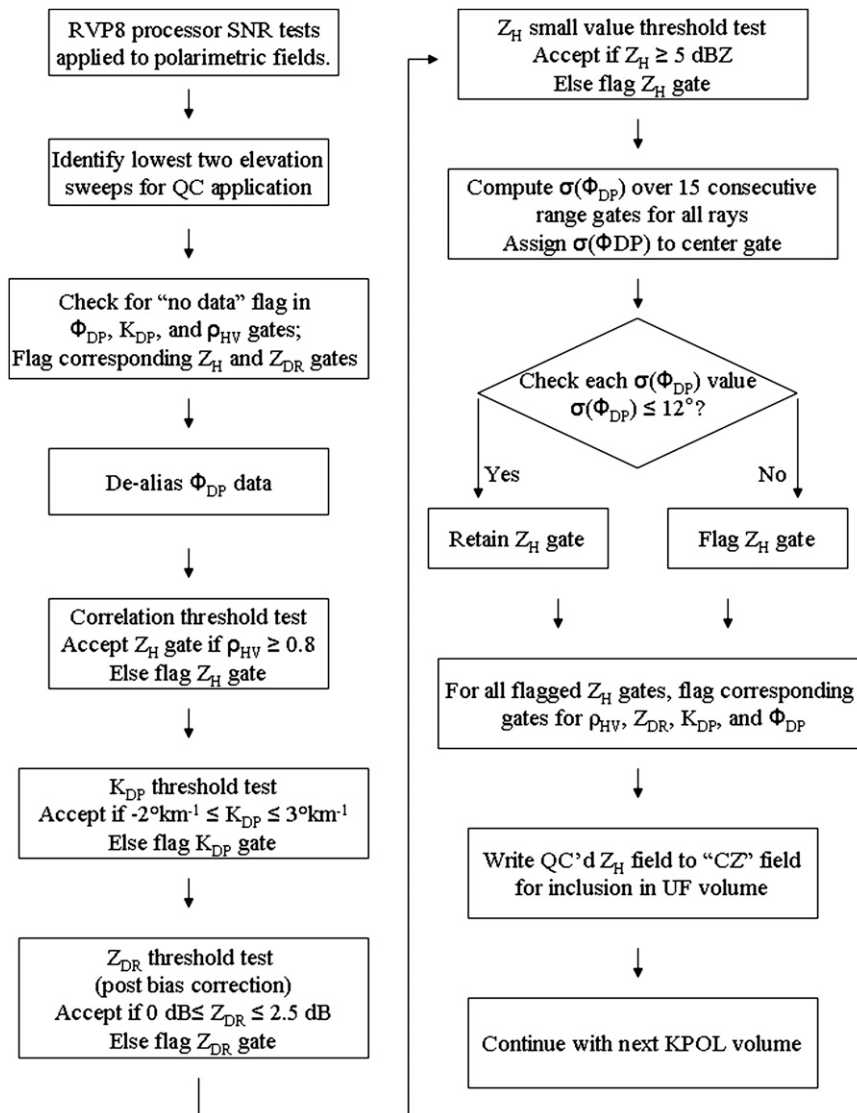


FIG. 2. KPOL quality control algorithm flowchart for the first two elevation angles. See text for explanation.

our DP QC algorithm, a new data field with the label “CZ” is created for each volume scan and contains the final precalibrated reflectivity that has been edited for suspected nonprecipitation echo. The first step in the DP QC process is automated and applied by the RVP8 processor. From the processor user’s manual (SIGMET RVP8 processor user’s manual is available from Vaisala online at <http://www.vaisala.com/weather/products/rvp8.html>), signal-to-noise ratio (SNR) tests (as currently configured at KPOL) are applied to the Φ_{DP} (PH), K_{DP} (KD), Z_{DR} (DR), and ρ_{HV} (RH) fields to identify gates with weak or uncertain signals, and the value of these gates are set to the no-data flag. Most multiple-trip echoes fail the KPOL-configured SNR tests within the Φ_{DP} , K_{DP} , and

ρ_{HV} fields, and are cleanly removed by the processor. The DP QC algorithm maps all of the gates containing the no-data flag within these fields to the corresponding Z_H and Z_{DR} gates, thereby eliminating almost all of the multiple-trip echoes.

The total differential phase (Φ_{DP}) contains both the radar system phase and a cumulative phase resulting from scattering from precipitation (Gorgucci et al. 1999; Bringi and Chandrasekar 2001). The KPOL system phase has a history of variation from near 0° to just under the maximum unambiguous value of 180° . As a consequence, the Φ_{DP} field has shown varying amounts of aliasing depending upon the data being analyzed. A gate is considered aliased if the absolute value of the phase difference between the

consecutive gates exceeds 149° . All of the aliased gates are corrected by adding 180° to the existing phase value.

An additional series of QC steps to test for typical values (in rain) and noise are applied to each gate of every ray from the ρ_{HV} , K_{DP} , and Z_{DR} fields. The specific thresholds applied in these tests are appropriate for KPOL observations. A simple correlation threshold test is employed, wherein gates are flagged if ρ_{HV} is less than 0.8. Correlation values within rain are considerably higher (greater than 0.9) and, therefore, the ρ_{HV} threshold of 0.8 is applied to distinguish between precipitation and clutter echoes.

The K_{DP} threshold test flags gates with values less than -2° km^{-1} or greater than $+3^\circ \text{ km}^{-1}$. The lower K_{DP} threshold was determined from empirical KPOL analysis of light rain under typical operating conditions. The upper K_{DP} threshold was determined from empirical analysis of the heaviest rain at Kwajalein (Z_H near 52 dBZ), wherein K_{DP} values do not exceed $2.4^\circ \text{ km}^{-1}$ as determined from analysis of both the radar and disdrometer data. The positive end of the K_{DP} allowed a range corresponding to a rain rate of $\sim 136 \text{ mm h}^{-1}$ using the $R(K_{DP})$ equation of Bringi and Chandrasekar (2001).

Analyses of Z_{DR} by the reflectivity interval (post-calibration) from the lowest two elevation sweeps indicate average values approaching 1–1.25 dB for the heaviest rain, which is similar to the Z_{DR} range computed from disdrometer observations (discussed in section 3a). For a primary application of quantitative rainfall estimation from the lowest elevations, the Z_{DR} test flags potential suspect gates with values less than 0 or greater than 2.5 dB. The lower Z_{DR} threshold for rain observations was based on theory from Doviak and Zrníc (1993, their Table 8.1), while the upper threshold was subjectively determined based on low-elevation KPOL observations under typical operating conditions. Although some light rain gates may be flagged because of the lower Z_{DR} threshold, qualitative analysis of the QCed Z_{DR} field suggests that this may be of minimal concern. A low-reflectivity threshold test is also employed, wherein Z_H gates with values less than 5 dBZ are flagged. The low Z_H value test is not a validity check, but it is needed as a matter of convenience because these gates are persistent in contaminating interpolated fields for rain-rate estimation.

The calculation of $\sigma(\Phi_{DP})$ and subsequent threshold testing is shown in Ryzhkov and Zrníc (1998b) to be a successful test for the detection of anomalous propagation (AP)-induced ground clutter echoes. The technique is also effective for *any* type of ground clutter or region of low SNR, and it has been applied to KPOL data for the identification of ground clutter from structures (i.e., buildings and towers). Robust QC results (described in the following section) indicate that 15 Φ_{DP} gates are sufficient for estimating the standard deviation. Using a

running centered 15-gate sample, $\sigma(\Phi_{DP})$ is computed at each range gate. If at least 5 of the 15 gates contain valid Φ_{DP} measurements, then their σ value is assigned to the center of the radial interval; otherwise, the σ value is set to the no-data flag. When $\sigma(\Phi_{DP})$ calculations are complete for a given sweep, each gate value is checked against an empirically determined threshold. If a $\sigma(\Phi_{DP})$ gate either is greater than the threshold or has been set to the no-data flag, then the corresponding Z_H gate is flagged. Within accumulating rain ($15 \text{ dBZ} \leq Z_H < 55 \text{ dBZ}$) the typically observed average $\sigma(\Phi_{DP})$ from KPOL is about 3° . Choosing a multiple of four, the threshold has been set to 12° for improved identification of AP (discussed in section 2c). In developing the DP QC algorithm, the sensitivity of multiple $\sigma(\Phi_{DP})$ thresholds was empirically checked. Although initially guided by theory (Ryzhkov and Zrníc 1998b), the choice of threshold in the final analysis was primarily empirical.

The final QC step maps flagged Z_H gates to the corresponding gates in ρ_{HV} , Z_{DR} , K_{DP} , and Φ_{DP} . The first two elevation sweeps are QCed in this manner. The Z_H field is then written to CZ for inclusion in the Universal Format (UF) volume.

c. QC results

Sea clutter, ground clutter from structures, and general noise are detected and eliminated by using a combination of $\sigma(\Phi_{DP})$ and ρ_{HV} thresholding. Analysis of ρ_{HV} within sea clutter reveals values that are mostly less than 0.40; however, values in the range from 0.0 to near 0.95 can occur. A similar analysis of $\sigma(\Phi_{DP})$ within sea clutter shows standard deviation values ranging from 3° to 70° . This wide range of correlation and standard deviation values is expected given the varying nature of returns from ocean waves. With a ρ_{HV} threshold of 0.80 and a $\sigma(\Phi_{DP})$ threshold of 12° , almost all of the sea clutter is detected. Echoes clearly identified as ground clutter from reflectivity time series analysis display typical ρ_{HV} values in the 0.4–0.95 range. More than 50% of these ground targets have ρ_{HV} values exceeding 0.80 and could easily be incorrectly identified as precipitation echoes if the correlation test was considered alone; therefore, the $\sigma(\Phi_{DP})$ test is also needed. Within ground clutter, $\sigma(\Phi_{DP})$ has values ranging from 10° to near 80° , with a clear majority of values greater than 40° . The combination of the correlation and standard deviation tests identifies almost all of the ground clutter gates; however, a small percentage of problem gates are not flagged by either threshold and survive the QC tests.

Figure 3 shows typical results of the RVP8 SNR tests and DP QC algorithm for the 0.4° elevation Z_H field. Figures 3a,b show raw and corrected reflectivity images within a 50-km radius and indicate the effective

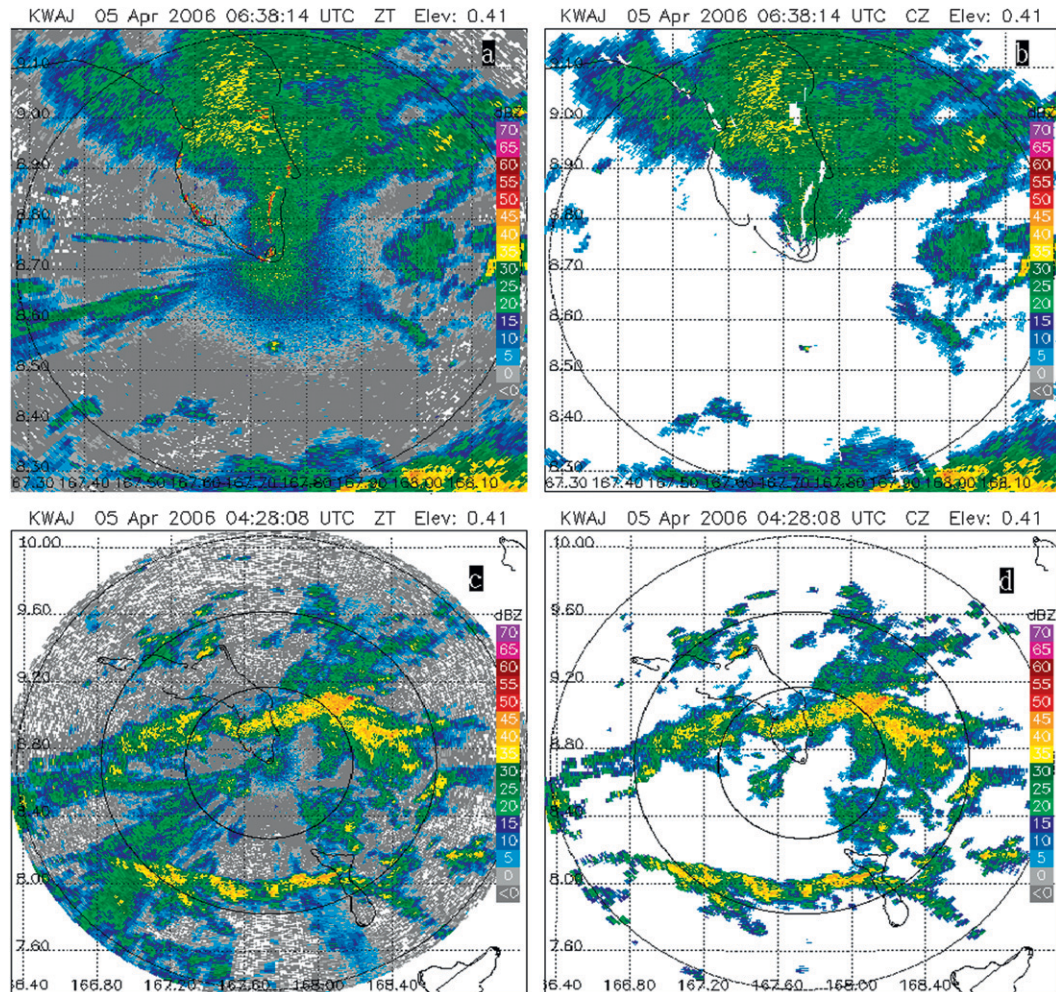


FIG. 3. Examples showing persistent ground clutter and multiple-trip echoes (a) in raw KPOL data (0638 UTC 5 Apr 2006 zoomed image with 50-km range ring), and (b) removal of the nonprecipitation echoes by the RVP processor SNR tests and the DP QC algorithm. (c) A raw 0.4° elevation sweep shows significant multiple-trip echoes (southwest of KPOL, 20–160-km range), ground and sea clutter, and typical noise (from 0428 UTC 5 Apr 2006). (d) The DP QC and processor corrected field shows dramatic improvement. Range rings are at 50-km intervals.

identification of multiple-trip echoes (by the SNR tests), sea clutter, and ground clutter along the atoll perimeter (both embedded and nonembedded) in precipitation. Figures 3c,d show a full 160-km, 0.4° elevation sweep before and after the SNR tests and DP QC. Pronounced regions of multiple-trip echoes (from 220° to 250°), ground clutter, and sea clutter have been removed in addition to widespread light noise.

The percentage of gates flagged as “bad” by each of the DP QC tests is shown in Table 6. Statistics are from the first two elevation sweeps, with a range of 0–100 km and 0° – 360° in azimuth, and were determined by comparison of the fields before and after DP QC. Within these elevation and range limits, we are well below the melting level and radar-observed bright band. The relatively high percentage of flagged gates for the Z_{DR} threshold test is

due to values less than 0 dB. Gates flagged in total reflectivity (ZT) includes those from the ρ_{HV} , $\sigma(\Phi_{DP})$, low Z_H threshold, and no-data tests from the DP fields. The ZT percentages vary significantly from case to case and are heavily influenced by flagging those gates less than 5 dBZ.

A quantitative comparison of the results from DP QC and legacy TRMM Ground Validation System (GVS) nonpolarimetric QC reveals notable differences. As discussed in Kulie et al. (1999), the GVS QC algorithm identifies nonprecipitation echo by use of height and reflectivity threshold parameters, and it has a significant weakness in removal of high-reflectivity ground clutter, especially when the clutter is near or embedded within precipitation. The strongest precipitation echoes at Kwajalein approach 52 dBZ, but ground clutter returns easily exceed this value with measurements

TABLE 6. DP QC algorithm results for each of the case studies. Statistics represent the maximum percentage of gates flagged as “bad” or “noise” by the individual tests from the first two elevation sweeps within each volume scan. Statistics are from the rainfall estimation range of 0–100 km and 0°–360° in azimuth, and were determined by comparing the final QC field with the initial non-QC field.

Case	ρ_{HV}	K_{DP}	Z_{DR}	$\sigma(\Phi_{DP})$	Total ZT
19 Dec 2006	3	1	17	2	5
3 Aug 2007	2	2	34	3	8
11 Aug 2007	8	3	30	6	29
19 Sep 2007	4	2	33	4	24
23 Nov 2007	5	2	23	7	29

ranging from 55 to 70 dBZ. Figure 4 shows the location of the clutter field at Kwajalein, with 1323 gates (within 50 km of KPOL) identified as frequent sources of clutter (Silberstein et al. 2008). Reflectivity gates are extracted exclusively from these clutter locations from unedited (raw) and corrected data from both DP and GVS QC algorithms for the five daily case studies. To be reasonably certain that no precipitation echo is selected, only reflectivity values ≥ 55 dBZ are considered to be ground clutter. Table 7 shows the gate count ≥ 55 dBZ from uncorrected, DP-corrected, and GVS-corrected data. The 19 December 2006 case shows that 71 gates from a total of 11 907 extracted gates have values ≥ 55 dBZ. DP QC has correctly identified and removed all 71 gates (100% correction); therefore, zero clutter gates remain. GVS QC has 53 remaining clutter gates ≥ 55 dBZ, roughly corresponding to a 25% correction. Similar results are shown for all cases. DP QC has eliminated most clutter gates, while GVS QC has a significant numbers of clutter gates remaining. In these cases, precipitation echo is widespread and ground clutter echo is mostly embedded in (or in close proximity to) precipitation echo. The DP QC tests (correlation and standard deviation of phase) detect and remove the embedded clutter, but GVS QC historically fails in this regard. In cases with partial precipitation coverage and nonembedded clutter, it is possible for marginal improvement of GVS QC performance through threshold strengthening, but it requires repetitive labor-intensive processing. In contrast, the DP QC algorithm is fully automated and provides consistent results without the necessity of parameter adjustments.

3. KPOL calibration

a. Differential reflectivity calibration

Accurate Z_{DR} calibration is an essential first step in the determination of absolute reflectivity calibration via consistency, and it is also critical for rain-rate estimation and hydrometeor identification. The use of vertically

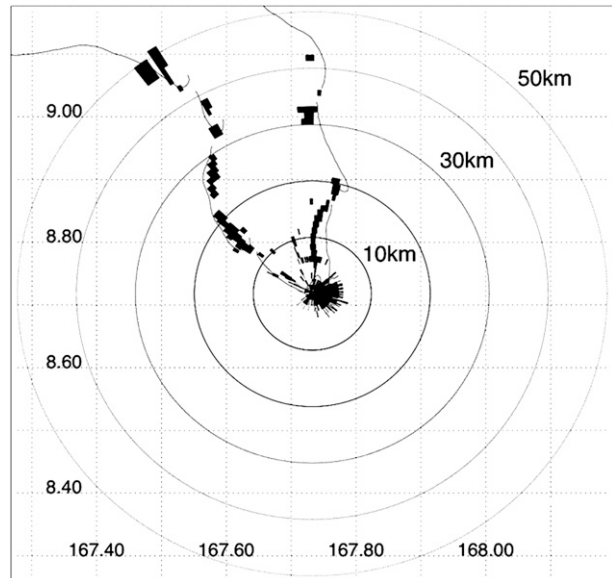


FIG. 4. Map of the clutter field at Kwajalein. Range rings are drawn at 10-km intervals from the radar site. (From Silberstein et al. 2008.)

pointing (or birdbath) observations in light rain is a favored and reliable approach to determine Z_{DR} bias (Gorgucci et al. 1999; Hubbert et al. 2008). The KPOL datasets from years 2006 and 2007 do not contain reliable vertical profiles; therefore, an alternative calibration method was needed for retroactive application. Although there are numerous methods described in the literature (Zrníc et al. 2006; Hubbert et al. 2003; Ryzhkov et al. 2005; Bechini et al. 2008), none are relevant or easily implemented because of operational limitations, hardware constraints, or data isolation and analysis issues.

The retroactive calibration of KPOL Z_{DR} was accomplished through bias adjustment to a disdrometer-determined Z_{DR} reference. Over 10 000 Joss–Waldvogel (JW) disdrometer observations of Z_H and Z_{DR} from 2003 and 2004 were compiled for this reference. The disdrometer was located at the KPOL site and recorded the entire spectrum of precipitation intensities. Assumptions regarding drop size and shape relations used in the disdrometer Z_{DR} computation are described in section 3b(1). KPOL Z_{DR} data from 2006 and 2007 (smoothed via a boxcar application)¹ were calibrated for individual rain events by applying specific offsets determined by

¹ Each Z_{DR} gate has been smoothed by a “boxcar” application. A smoothed gate is defined as the average Z_{DR} value from five gates (i.e., a specific gate and the four surrounding gates). The four surrounding gates are defined as 1) the next gate in the same ray, 2) the previous gate in the same ray, 3) the corresponding gate from the next ray, and 4) the corresponding gate from the previous ray. More information can be obtained from Bringi and Thurai (2008).

TABLE 7. Comparison of DP QC and nonpolarimetric TRMM GVS QC results with respect to ground clutter detection. Raw reflectivity data were extracted from locations with frequent ground clutter echoes. The gate count represents the remaining gates considered to be ground clutter after QC is applied. For this study, gates ≥ 55 dBZ are considered ground clutter. DP QC shows superior performance as compared to the nonpolarimetric (TRMM GVS) QC as evidenced by the low gate counts.

Case	Number of unedited gates ≥ 55 dBZ/ total extracted gates	DP QC			GVS QC		
		Gate count ≥ 55 dBZ	≥ 60	≥ 65	Gate count ≥ 55 dBZ	≥ 60	≥ 65
19 Dec 2006	71/11907	0	0	0	53	3	0
3 Aug 2007	237/35721	3	0	0	193	45	0
11 Aug 2007	383/15720	0	0	0	85	31	0
19 Sep 2007	137/18522	0	0	0	111	28	0
23 Nov 2007	528/18429	9	1	0	478	166	34

comparison to the disdrometer reference. Before determining the proper Z_{DR} offset, the Z_H distributions were independently calibrated by the relative calibration adjustment (RCA) method [further details are available in section 3b(2) (see Silberstein et al. 2008; Marks et al. 2009)]. The Z_{DR} – Z_H disdrometer reference is shown in the top panel of Fig. 5 (bold line with no symbols), together with observations from the five case studies. The level of disagreement in Z_{DR} distributions within the cases is evident, and their bias relative to the disdrometer reference is shown in the legend. Fluctuations in Z_{DR} bias of 0.1 to 0.2 dB were common prior to electrical upgrades in early 2008. The bottom panel of Fig. 5 shows the Z_{DR} distributions after adjustment to the reference, and the standard deviation error bars from both instruments. The KPOL standard deviations are from the 3 August 2007 case and are representative of the standard deviations from all of the cases.

Emphasis was placed on matching Z_{DR} within the 30–40-dBZ range because this represents approximately 85%–90% of the measurements used in self-consistency calibration. While the adjusted Z_{DR} measurements are not in perfect agreement, and fluctuations resulting from sample size limitations are noticeable especially in the upper reflectivity intervals, our analysis indicates that the agreement is sufficient to perform a robust calibration of Z_H using the self-consistency technique. After Z_{DR} offsets were determined, the RCA-adjusted Z_H values were no longer used. The self-consistency calibration of Z_H (described in the following section) is completely independent of the RCA-adjusted data and method.

Measurements of Z_{DR} in light rain with the antenna vertically pointed (at a 90° elevation angle) commenced in March 2008 and have continued through 2009. Results consistently show that the Z_{DR} values are too high (“hot”) by approximately 1.0 dB. Electrical upgrades and calibration efforts resulted in the Z_{DR} bias change from 2007 to 2008. Figure 6 displays vertical profile measurements from 25 September 2008 during a shallow light rain event. The vertical profile of mean Z_{DR} (top right panel) shows bias of approximately +1 dB near the 3.0-km level.

The mean ρ_{HV} values near 0.99 are indicative of sampling in the rain medium (lower left panel). A 2.8-km mean Z_{DR} distribution by azimuth (bottom right panel) shows the periodic nature of the direction-dependent measurements, which is an expected structure resulting from variability in the ground clutter response from sidelobes with antenna rotation in the vertical (Gorgucci et al. 1999). Here, Z_{DR} is averaged from the full azimuth cycle of 360° , over which 1023 samples per azimuth are obtained. For comparison of the birdbath and disdrometer reference methods, the mean birdbath-adjusted Z_{DR} and standard deviation (by reflectivity interval) for data nearly concurrent with the 25 September 2008 case are plotted in the bottom panel of Fig. 5 (bold dashed line with smallest endcaps). For this case, the mean Z_{DR} values between the two methods are very comparable, with slightly larger standard deviations for the birdbath case.

b. Self-consistency calibration: Methodology and results

1) METHODOLOGY

Polarimetric properties of the rain medium can be used to determine the absolute calibration of a radar system. Techniques used to capitalize on these consistency relations range from the comparison of rainfall rates derived from power and phase measurements (Gorgucci et al. 1992) to the comparison of the observed and estimated differential propagation phase (Goddard et al. 1994; Vivekanandan et al. 2003; Ryzhkov et al. 2005, and others). The self-consistency of Z_H , Z_{DR} , and K_{DP} measurements was quantified by Scarchilli et al. (1996) and Gorgucci et al. (1999) using a gamma distribution model. The majority of these self-consistency calibration techniques have a common necessity of heavy rain rates (greater than 50 mm h^{-1}) for significant phase accumulation at S band over the range profile. Ryzhkov et al. (2005) suggested a methodology for determining absolute reflectivity bias (Z_{BIAS}) from the self-consistency relation that did not require heavy rainfall at S band. This methodology compared area–time integrals of measured

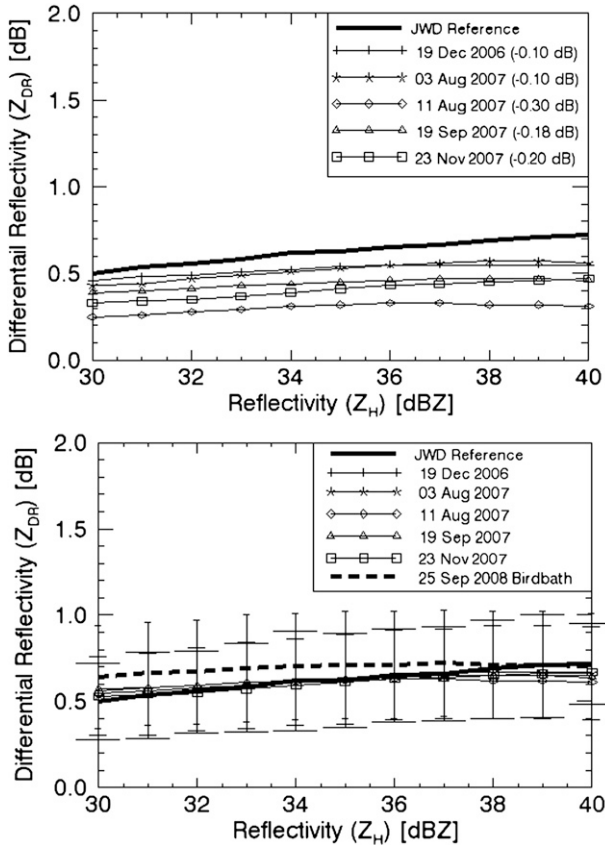


FIG. 5. Distribution of average Z_{DR} measurements by reflectivity interval. (top) The unadjusted Z_{DR} curves show the bias in five case studies relative to the JW disdrometer Z_{DR} reference (bold, no-symbol line). Biases are shown in the legend. (bottom) The Z_{DR} distributions bias adjusted to the disdrometer reference. The Z_{DR} standard deviation error bars for the disdrometer (longest endcaps) and KPOL (midsized endcaps) are very similar in this data range. The KPOL standard deviations are from the 3 Aug 2007 case and are representative of the standard deviations from all five case studies. For comparison, the 25 Sep 2008 (birdbath adjustment method) average Z_{DR} and standard deviations are shown by the heavy dashed line and smallest endcaps (reference Fig. 6 and associated text); Z_H distributions have been calibration corrected via the independent RCA method.

(processor or user determined) K_{DP} and estimated (theoretical) K_{DP} as a function of Z_H and Z_{DR} . The Z_{BIAS} was then quantified as the adjustment in Z_H needed for the integrals to agree. This K_{DP} -based method was chosen for application to KPOL data because of the predominant nature of light rain events.

The precipitation at Kwajalein is dominated by systems that form in the intertropical convergence zone (ITCZ), as well as shallow (less than 5 km) “warm rain” clouds (Schumacher and Houze 2000; Wolff et al. 2005), and it is ideal for self-consistency calibration because of this lighter rain regime. To apply the area integration methodology to KPOL data, DSD measurements from

Kwajalein were required to derive a consistency equation between Z_H , Z_{DR} , and K_{DP} . Using simulated DSD, Vivekanandan et al. (2003) derived a relationship where K_{DP} is expressed as a function of Z_H and Z_{DR} . In our study, we derived a similar relation using actual disdrometer observations. A JW disdrometer sited at Kwajalein from May through December 2003 provided 8779 one-minute resolution DSD measurements (within the 30–48-dBZ interval) to regress the following relation between the variables:

$$K_{DP} = AZ_H^b Z_{DR}^c. \quad (4)$$

The polarimetric radar parameters of Z_H , Z_{DR} , and K_{DP} were calculated for each minute of DSD observations for an S-band radar (10.7 cm) and a temperature of 20°C, as shown in Tokay et al. (2002). For drop shape, the mean axis ratios offered by Andsager et al. (1999) were adopted for drops less than 4 mm in diameter and equilibrium drop shapes (Beard and Chuang 1987) for larger drops. For the fall velocity, we adopted the terminal fall velocity drop diameter relation given by Beard (1976). The coefficient and exponents were derived via a linear least squares fit regression ($A = 0.17737 \times 10^{-4}$, $b = 0.9926$, and $c = -0.5138$) with Z_H ($\text{mm}^6 \text{m}^{-3}$), Z_{DR} (dB), and K_{DP} ($^\circ \text{km}^{-1}$).

Following the Ryzhkov et al. (2005) method, we matched the measured K_{DP} and estimated $K_{DP}(Z_H, Z_{DR})$ by adjusting Z_H by an amount (dB) considered as the Z_{BIAS} . A practical approach to accomplish this is to divide the data collected from an entire spatial/temporal domain into 1-dB increments of radar reflectivity and compute average values of $K_{DP}(Z)$ and $Z_{DR}(Z)$ within each 1-dB interval of Z between Z_{\min} (30 dBZ) and Z_{\max} (48 dBZ). The Z_{BIAS} is then determined by matching the summations

$$I_1 = \sum_{Z_{\min}}^{Z_{\max}} \overline{K_{DP}(Z)} n(Z) \Delta Z \quad (5)$$

and

$$I_2 = A \sum_{Z_{\min}}^{Z_{\max}} Z_H^b \overline{Z_{DR}(Z)}^c n(Z) \Delta Z, \quad (6)$$

where $n(Z)$ is the number of gates within each 1-dB interval. The initial estimated Z_{BIAS} is determined from Vivekanandan et al. (2003) by

$$Z_{BIAS}(\text{dB}) = 10 \log \left(\frac{I_2}{I_1} \right). \quad (7)$$

The initial Z_{BIAS} is applied to the reflectivity field, and Eqs. (5), (6), and (7) are then recomputed to determine

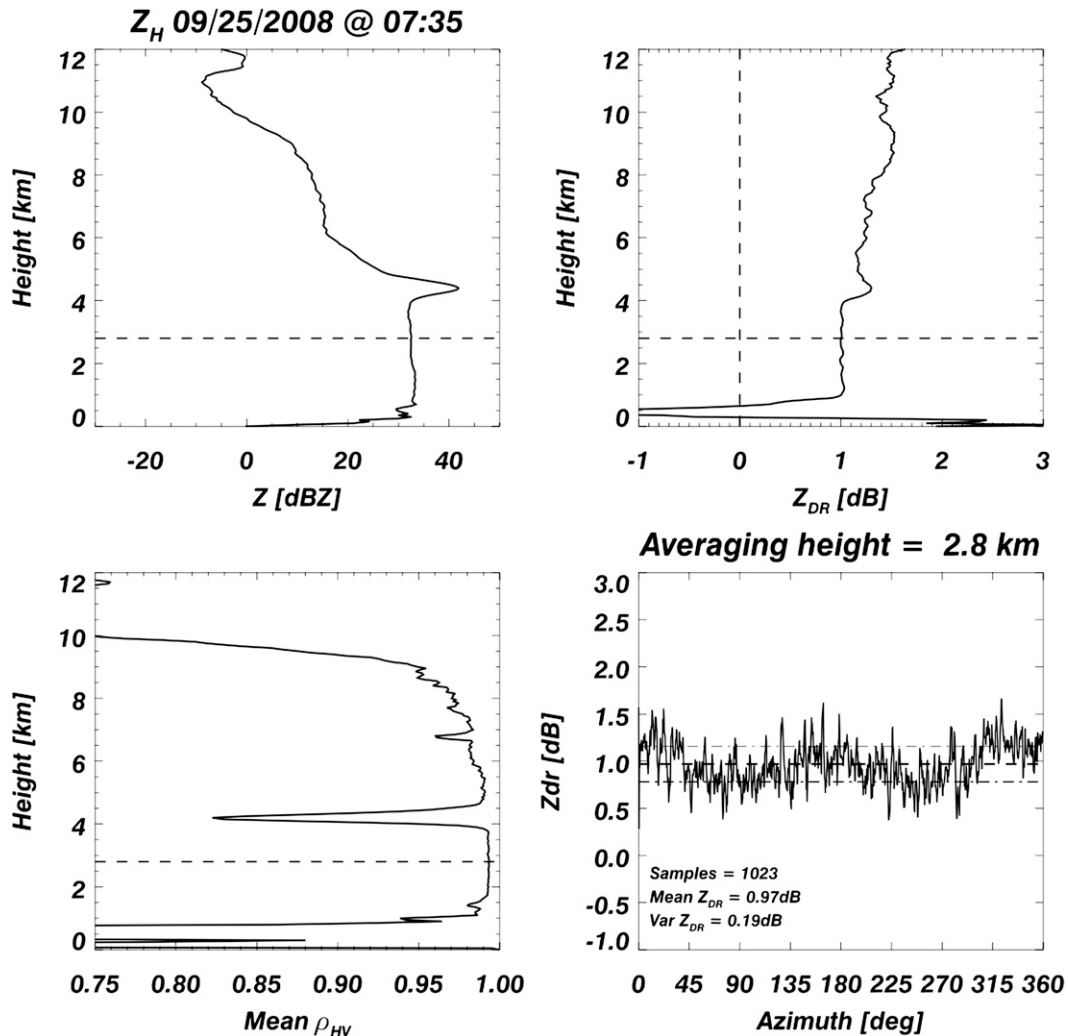


FIG. 6. Measurements of (top left) reflectivity with height, (top right) mean Z_{DR} with height, (bottom left) correlation with height, and (bottom right) mean Z_{DR} measurements with azimuth for a shallow light rain event at Kwajalein from 25 Sep 2008. The correlation profile indicates sampling in the rain medium near 3.0-km height. The azimuth measurements (bottom right) show the influence of directional-dependent response. The mean Z_{DR} bias of +0.97 dB (heavy dashed lined) was determined over the full azimuth cycle. The dash-dot lines represent one standard deviation.

ΔZ_{BIAS} [from Eq. (7)]. If the resulting ΔZ_{BIAS} is greater than 0.1 dB, it is again applied to the reflectivity field. The final Z_{BIAS} is the sum of the initial and iterated ΔZ_{BIAS} . Iteration is needed because we are subsampling the data in a Z_H range, and yet we are adjusting Z_H as part of the procedure. As a result, we effectively “shift” the sample of (Z_H, Z_{DR}, K_{DP}) triplets being used in the procedure as we adjust Z_H in each pass. One or two iterations are needed to force the agreement of (5) and (6), thereby reducing the ΔZ_{BIAS} to 0.1 dB. The final Z_{BIAS} value represents the absolute Z_H calibration adjustment needed for consistency between the polarimetric variables. The same cases analyzed for QC

and Z_{DR} calibration were examined for self-consistency calibration.

2) RESULTS

As a basis for evaluation, the self-consistency results are compared against those from the independent non-DP RCA technique (Silberstein et al. 2008).² The RCA uses a frequency distribution of reflectivity values from

² The RCA-adjusted Z_H reflectivity values are *not* used in any way in the self-consistency calibration method. The RCA is a completely independent statistical calibration approach.

TABLE 8. Self-consistency-derived calibration adjustments as compared with the independent RCA approach, and the absolute value of their difference. Shown is the cumulative number of K_{DP} samples compared (measured and derived via consistency) from the reflectivity intervals in the Z_{min} (30 dBZ) to Z_{max} (48 dBZ) range.

Case	K_{DP} samples	Self-consistency calibration Z_{BIAS} (dB)	RCA (dB)	Difference (dB)
19 Dec 2006	546434	-2.44	-1.95	0.49
3 Aug 2007	1521223	-2.06	-1.78	0.28
11 Aug 2007	335658	-1.46	-1.91	0.45
19 Sep 2007	400012	-0.93	-1.91	0.98
23 Nov 2007	740603	-2.17	-2.46	0.29

persistent ground clutter areas from every volume scan to monitor hourly and daily radar sensitivity changes relative to an established baseline. A practical application of the RCA technique to KPOL data revealed a dramatic improvement in data stability as evidenced by reflectivity comparisons with the TRMM precipitation radar (PR). Although the RCA provides a relative calibration, corrected KPOL reflectivity matched the PR to within ± 1 dB on a monthly and yearly basis (Marks et al. 2009; Wang and Wolff 2009). Table 8 shows self-consistency calibration results as compared to the RCA approach and the absolute value of their difference. From the case studies analyzed, there is agreement between self-consistency and RCA to within ± 1 dB. In four cases, the agreement is within 0.5 dB. These results are similar to Ryzhkov et al. (2005) upon comparison of corrected reflectivity with independent measurements. Illingworth and Blackman (2002) and Vivekanandan et al. (2003) have also determined that the accuracy of generally similar self-consistency calibration can be as good as 0.5–1 dB as evaluated through independent comparison. The KPOL results are consistent with previous calibration studies and provide confidence in the self-consistency method.

The consistency relationship given by (4) was derived from disdrometer observations at Kwajalein and, therefore, the relationship can serve as an empirical reference for verification of the self-consistency method after bias correction. Figure 7 shows comparisons between average K_{DP} measurements (after Z_{BIAS} correction) and those calculated from self-consistency [$K_{DP}(Z_H, Z_{DR})$]. There is reasonable agreement between the profiles (with the 11 August 2007 and 23 November 2007 cases as exceptions). A noticeable disagreement in profiles is apparent at both lower and upper ends of the reflectivity range. From approximately 30 to 35 dBZ, RVP8-calculated K_{DP} is higher than consistency theory (Z_H, Z_{DR} empirical reference). This could be due to difficulty in extracting the

true K_{DP} signal (less than $0.1^\circ \text{ km}^{-1}$) from the embedded noise field despite substantial sample size and extensive averaging. The agreement is best within the 35–43-dBZ range, which is attributed to a stronger K_{DP} signal and sufficient sample sizes. In reflectivity intervals greater than 43 dBZ, the radar-measured K_{DP} falls lower than the reference in all cases. The number of independent K_{DP} samples in reflectivity intervals from 43 to 48 dBZ is significantly lower than in the other intervals (< 500 from the 19 December 2006 case; see Table 5). Probability distribution functions show that in all cases, approximately 95% of the K_{DP} values within the distribution are accounted for within the 30–43-dBZ range. This result is not surprising because of the predominant occurrence of lower reflectivity precipitation at Kwajalein. These calibration results are obviously weighted with the majority of the samples; therefore, not much significance can be placed on the results from the higher reflectivity intervals.

Other explanations for disagreement in profiles at the lower and upper ends of the reflectivity range could be related to possible bias in the disdrometer-derived consistency equation and the effects of processor filtering of differential phase for K_{DP} calculation. The relatively poor agreement in the 11 August 2007 and 23 November 2007 cases is likely related to the nature of the precipitation itself. As compared to the other cases, there is significantly more convection present and the echo shields display less of a uniform coverage pattern. This self-consistency method does not appear to be applicable to cases with numerous convective cells or scattered showers. The most favorable results are from cases with uniform, widespread, light rain shields. This finding is consistent with either 1) the calibration bias [Eq. (4)] being tuned to lighter rain DSDs (versus more convective, heavier rain DSDs) and/or 2) challenges in estimating K_{DP} in small, isolated convective cells. The calibration results presented in Table 8 and Fig. 7 provide further confirmation of the Ryzhkov et al. (2005) method and show that an absolute bias adjustment to Z_H can be determined by matching K_{DP} profiles in relatively light rain, provided a local consistency relationship is available.

4. Summary and discussion

The development and adaptation of algorithms for QC and reflectivity calibration have been initiated in an oceanic environment with DP observations from KPOL. Presented are algorithms for DP QC and absolute reflectivity calibration using polarimetric properties of the rain medium. Application of the DP QC algorithm has shown to be robust with superior results compared to the TRMM GV (nonpolarimetric) QC algorithm that

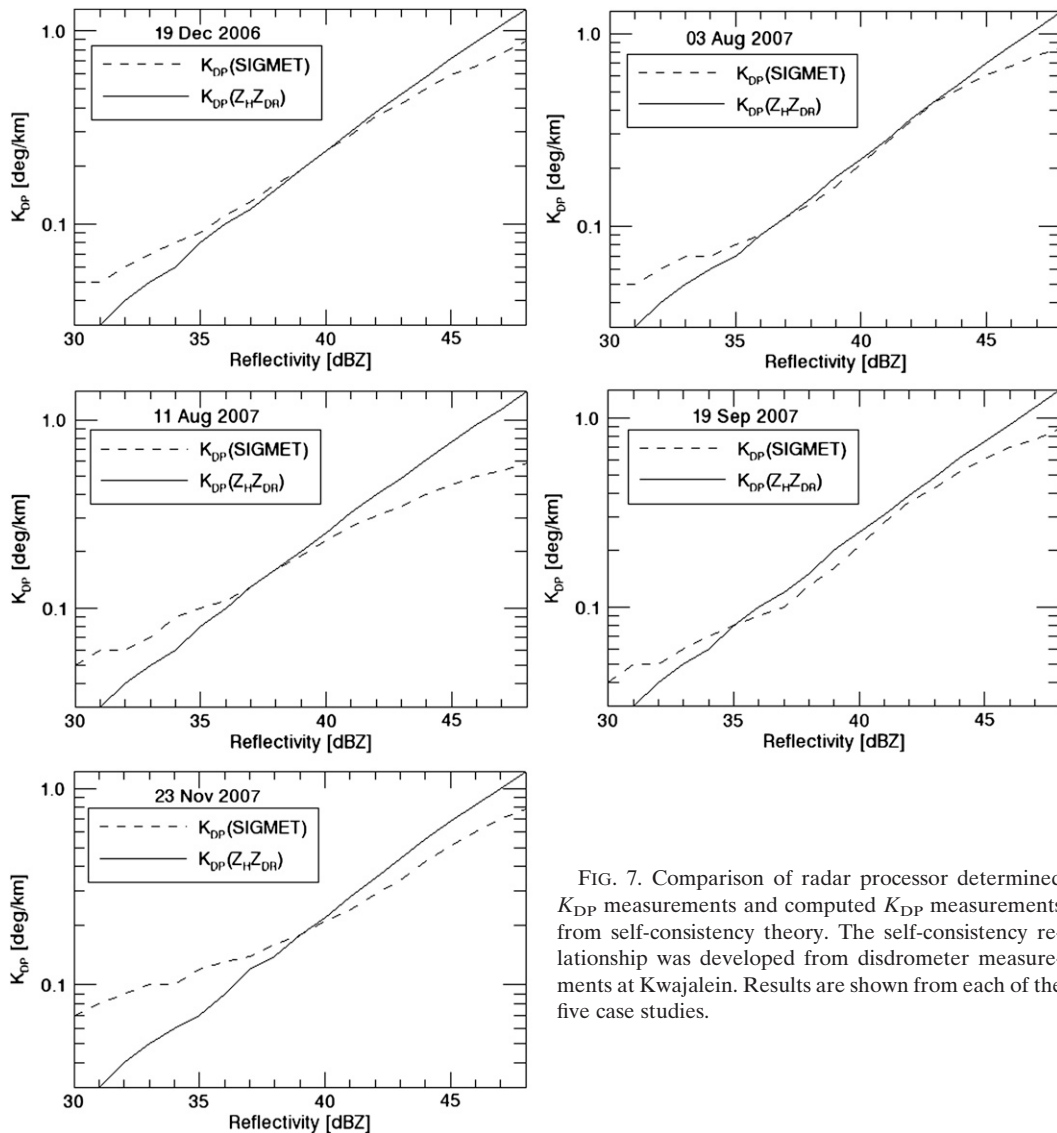


FIG. 7. Comparison of radar processor determined K_{DP} measurements and computed K_{DP} measurements from self-consistency theory. The self-consistency relationship was developed from disdrometer measurements at Kwajalein. Results are shown from each of the five case studies.

employs height and reflectivity thresholds. The ability to detect and remove ground and sea clutter embedded in precipitation echo is a distinct advantage of the DP algorithm. Through the application of thresholding tests for the correlation and standard deviation of differential phase, almost all clutter-type returns are identified and removed. In contrast, the TRMM GV algorithm can remove ground clutter only when not embedded in precipitation and can be a labor-intensive process. In addition, the RVP8 processor correctly identifies and removes multiple-trip echoes through automated SNR power tests (as currently configured at KPOL), a successful result to which the DP QC algorithm takes full advantage.

A technique for determining retroactive Z_{DR} calibration through the analysis of combined Z_{DR} and Z_H observations was developed and applied to KPOL data.

This application adjusts Z_{DR} observations to match a disdrometer distribution when vertical profile measurements are not available. By this technique, uncertainty has been mitigated in Z_{DR} data from significant rainfall events in 2006 and 2007 and has allowed the application of self-consistency reflectivity calibration.

A phase-based self-consistency approach used to determine absolute reflectivity calibration using properties of the rain medium in light rain has been tested with KPOL data from five case studies and found to provide good results (within ± 1.0 dB) as compared to the independent RCA method. The approach follows the work of Ryzhkov et al. (2005) where K_{DP} data from light rain events are integrated and compared against a consistency equation derived from disdrometer data at Kwajalein. In lower reflectivity intervals (30–35 dBZ), the observed

K_{DP} measurements indicate a high bias relative to the disdrometer-based reference, possibly resulting from difficulty in extracting the true K_{DP} signal. In midreflectivity intervals (35–43 dBZ), there is reasonable agreement between observed and consistency-derived K_{DP} profiles. Differences may be related to possible bias in the disdrometer-derived consistency equation and the assumptions from which it was derived. The results indicate that the method can be successfully applied to lighter precipitation regimes. The most favorable results were found in cases with widespread, uniform, light rain shields.

The Ryzhkov et al. (2005) consistency calibration method was developed with polarimetric observations from central Oklahoma. In our study, we present another careful test of Ryzhkov et al. (2005) from a very different meteorological regime. The encouraging results increase confidence that the technique might have a future in near-real-time operations for at least TRMM and GPM GV with WSR-88D radars from many environments (Morris and Schwaller 2009), but that the application and resulting interpretation may need expert user oversight. It is not clear at this time if future baseline WSR-88D DP data made available to the community by the National Oceanic and Atmospheric Administration (NOAA) will have sufficient calibration for research applications. For certain, NASA's PMM GV programs will require continued verification of WSR-88D calibration using all available means, and the results of this study suggest that the consistency method of Ryzhkov et al. (2005), and possibly the RCA method of Silberstein et al. (2008), may be viable options for select radars at a minimum.

DP radars will certainly be a vital tool for GPM validation because of their applications to rainfall microphysical retrievals (Chandrasekar et al. 2008). Through the retrieval of DSD parameters relating drop size and shape, rainfall estimation, and hydrometeor identification, DP radars can provide validation of parameterized microphysical properties. The ability to provide consistent and long-term QCed and calibrated ground-based DP measurements will prove essential for calibration of the core GPM satellite and for development of physically based passive microwave radiometer algorithms.

Acknowledgments. This research is supported by NASA Grant NNG07EJ50C. The authors thank Dr. Ramesh Kakar (NASA Headquarters), Dr. Arthur Hou (GPM Project Scientist, NASA/GSFC), Dr. Scott Braun (TRMM Project Scientist, NASA/GSFC), and Dr. Mathew Schwaller (GPM GV Program Manager, NASA/GSFC) for their support of this effort. Appreciation is extended to David Silberstein for numerous helpful discussions, and to the TRMM Satellite Validation Office

staff, including Bart Kelley, Jason Pippitt, David Makofski, and Jianxin Wang. CSU–CHILL data were provided by Patrick Kennedy of Colorado State University. NCAR S-Pol data were provided by the NCAR ATD. We thank the staff of Atmospheric Technology Services Company for providing KPOL data.

REFERENCES

- Andsager, K., K. V. Beard, and N. F. Laird, 1999: Laboratory measurements of axis ratios for large raindrops. *J. Atmos. Sci.*, **56**, 2673–2683.
- Balakrishnan, N., and D. S. Zrnic, 1989: Correction of propagation effects at attenuating wavelengths in polarimetric radars. Preprints, *24th Conf. on Radar Meteorology*, Tallahassee, FL, Amer. Meteor. Soc., 287–291.
- Beard, K. V., 1976: Terminal velocity and shape of cloud and precipitation drops aloft. *J. Atmos. Sci.*, **33**, 851–864.
- , and C. Chuang, 1987: A new model for the equilibrium shape of drops. *J. Atmos. Sci.*, **44**, 1509–1524.
- Bechini, R., L. Baldini, R. Cremonini, and E. Gorgucci, 2008: Differential reflectivity calibration for operational radars. *J. Atmos. Oceanic Technol.*, **25**, 1542–1555.
- Bringi, V. N., and V. Chandrasekar, 2001: *Polarimetric Doppler Weather Radar—Principles and Applications*. Cambridge University Press, 636 pp.
- , and M. Thurai, 2008: Internal report for BMRC-BOM on the preliminary assessment and analysis of CP2 S and X band data. 6 pp.
- Brunkow, D., V. N. Bringi, P. C. Kennedy, S. A. Rutledge, V. Chandrasekar, E. A. Mueller, and R. K. Bowie, 2000: A description of the CSU–CHILL National Radar Facility. *J. Atmos. Oceanic Technol.*, **17**, 1596–1608.
- Carey, L. D., S. A. Rutledge, D. A. Ahijevych, and T. D. Keenan, 2000: Correcting propagation effects in C-band polarimetric radar observations of tropical convection using differential propagation phase. *J. Appl. Meteor.*, **39**, 1405–1433.
- Chandrasekar, V., A. Hou, E. Smith, V. N. Bringi, S. A. Rutledge, E. Gorgucci, W. A. Petersen, and G. S. Jackson, 2008: Potential role of dual-polarization radar in the validation of satellite precipitation measurements. *Bull. Amer. Meteor. Soc.*, **89**, 1127–1145.
- Cifelli, R., W. A. Petersen, L. D. Carey, S. A. Rutledge, and M. A. F. da Silva Dias, 2002: Radar observations of the kinematic, microphysical, and precipitation characteristics of two MCSs in TRMM LBA. *J. Geophys. Res.*, **107**, 8077, doi:10.1029/2000JD000264.
- Doviak, R. J., and D. S. Zrnic, 1993: *Doppler Radar and Weather Observations*. 2nd ed. Academic Press, 562 pp.
- Goddard, J., J. Tan, and M. Thurai, 1994: Technique for calibration of meteorological radars using differential phase. *Electron. Lett.*, **30**, 166–167.
- Gorgucci, E., G. Scarchilli, and V. Chandrasekar, 1992: Calibration of radars using polarimetric techniques. *IEEE Trans. Geosci. Remote Sens.*, **30**, 853–858.
- , —, and —, 1999: A procedure to calibrate multiparameter weather radar using properties of the rain medium. *IEEE Trans. Geosci. Remote Sens.*, **34**, 269–276.
- , —, —, and V. N. Bringi, 2001: Rainfall estimation from polarimetric radar measurements: Composite algorithms immune to variability in raindrop shape-size relation. *J. Atmos. Oceanic Technol.*, **18**, 1773–1786.

- Gosset, M., 2004: Effect of nonuniform beam filling on the propagation of radar signals at X-band frequencies. Part II: Examination of differential phase shift. *J. Atmos. Oceanic Technol.*, **21**, 358–367.
- Houze, R. A., Jr., S. Brodzik, C. Schumacher, and S. Yuter, 2004: Uncertainties in oceanic radar rain maps at Kwajalein and implications for satellite validation. *J. Appl. Meteor.*, **43**, 1114–1132.
- Hubbert, J. C., V. N. Bringi, and D. Brunkow, 2003: Studies of the polarimetric covariance matrix. Part I: Calibration methodology. *J. Atmos. Oceanic Technol.*, **20**, 696–706.
- , F. Pratte, M. Dixon, and R. Rilling, 2008: The uncertainty of Zdr calibration. Preprints, *Fifth European Conf. on Radar in Meteorology and Hydrology (ERAD 2008)*, Helsinki, Finland, Finnish Meteorological Institute. [Available online at <http://erad2008.fmi.fi/proceedings/extended/erad2008-0285-extended.pdf>.]
- Illingworth, A., and T. Blackman, 2002: The need to represent raindrop size spectra as normalized Gamma distributions for the interpretation of polarization radar observations. *J. Appl. Meteor.*, **41**, 286–297.
- Istok, M. J., and Coauthors, 2009: WSR-88D dual polarization initial operational capabilities. Preprints, *25th Conf. on Interactive Information and Processing Systems for Meteorology, Oceanography, and Hydrology*, Phoenix, AZ, Amer. Meteor. Soc., 15.5. [Available online at <http://ams.confex.com/ams/pdfpapers/148927.pdf>.]
- Kulie, M. S., M. Robinson, D. A. Marks, B. S. Ferrier, D. Rosenfeld, and D. B. Wolff, 1999: Operational processing of ground validation data for the Tropical Rainfall Measuring Mission. Preprints, *29th Int. Conf. on Radar Meteorology*, Montreal, QC, Canada, Amer. Meteor. Soc., 736–739.
- Kummerow, C., and W. A. Petersen, 2006: GPM ground validation: Strategy and efforts. NASA Global Precipitation Measurement, 14 pp. [Available online at http://gpm.gsfc.nasa.gov/images/webdoc2_gv_whitepaper.pdf.]
- Lutz, J., P. Johnson, B. Lewis, E. Loew, M. Randall, and J. VanAndel, 1995: NCAR's S-Pol: Portable polarimetric S-band radar. Preprints, *Ninth Conf. on Meteorological Observations and Instrumentation*, Charlotte, NC, Amer. Meteor. Soc., 408–410.
- Marks, D. A., D. B. Wolff, D. S. Silberstein, A. Tokay, J. L. Pippitt, and J. Wang, 2009: Availability of high-quality TRMM ground validation data from Kwajalein, RMI: A practical application of the relative calibration adjustment technique. *J. Atmos. Oceanic Technol.*, **26**, 413–429.
- Morris, K. R., and M. R. Schwaller, 2009: An enhanced Global Precipitation Measurement (GPM) validation network prototype. Preprints, *34th Conf. on Radar Meteorology*, Williamsburg, VA, Amer. Meteor. Soc., P7.3. [Available online at <http://ams.confex.com/ams/pdfpapers/155254.pdf>.]
- Ryzhkov, A. V., 2007: The impact of beam broadening on the quality of radar polarimetric data. *J. Atmos. Oceanic Technol.*, **24**, 729–744.
- , and D. S. Zrnica, 1998a: Discrimination between rain and snow with a polarimetric radar. *J. Appl. Meteor.*, **37**, 1228–1240.
- , and —, 1998b: Polarimetric rainfall estimation in the presence of anomalous propagation. *J. Atmos. Oceanic Technol.*, **15**, 1320–1330.
- , and —, 1998c: Beamwidth effects on the differential phase measurements of rain. *J. Atmos. Oceanic Technol.*, **15**, 624–634.
- , S. E. Giangrande, V. M. Melnikov, and T. J. Schuur, 2005: Calibration issues of dual-polarization radar measurements. *J. Atmos. Oceanic Technol.*, **22**, 1138–1154.
- Sachidananda, M., and D. S. Zrnica, 1985: ZDR measurement considerations for a fast scan capability radar. *Radio Sci.*, **20**, 907–922.
- Sarchilli, G., E. Gorgucci, V. Chandrasekar, and A. Dobaie, 1996: Self-consistency of polarization diversity measurement of rainfall. *IEEE Trans. Geosci. Remote Sens.*, **34**, 22–26.
- Schumacher, C., and R. A. Houze Jr., 2000: Comparison of radar data from the TRMM satellite and Kwajalein oceanic validation site. *J. Appl. Meteor.*, **39**, 2151–2164.
- Silberstein, D. S., D. B. Wolff, D. A. Marks, D. Atlas, and J. L. Pippitt, 2008: Ground clutter as a monitor of radar stability at Kwajalein, RMI. *J. Atmos. Oceanic Technol.*, **25**, 2037–2045.
- Straka, J. M., D. S. Zrnica, and A. V. Ryzhkov, 2000: Bulk hydrometeor classification and quantification using polarimetric radar data: Synthesis of relations. *J. Appl. Meteor.*, **39**, 1341–1372.
- Tokay, A., A. Kruger, W. Krajewski, P. A. Kucera, and A. J. Pereira Filho, 2002: Measurements of drop size distribution in the southwestern Amazon basin. *J. Geophys. Res.*, **107**, 8052, doi:10.1029/2001JD000355.
- Vivekanandan, J., D. S. Zrnica, S. M. Ellis, R. Oye, A. V. Ryzhkov, and J. Straka, 1999: Cloud microphysics retrieval using S-band dual-polarization radar measurements. *Bull. Amer. Meteor. Soc.*, **80**, 381–388.
- , G. Zhang, S. Ellis, D. Rajopadhyaya, and S. Avery, 2003: Radar reflectivity calibration using differential propagation phase measurement. *Radio Sci.*, **38**, 8049, doi:10.1029/2002RS002676.
- Wang, J., and D. B. Wolff, 2009: Comparisons of reflectivities from the TRMM Precipitation Radar and ground-based radars. *J. Atmos. Oceanic Technol.*, **26**, 857–875.
- Wang, J. J., and L. D. Carey, 2005: The development and structure of an oceanic squall-line system during the South China Sea Monsoon Experiment. *Mon. Wea. Rev.*, **133**, 1544–1561.
- Wolff, D. B., D. A. Marks, E. Amitai, D. S. Silberstein, B. L. Fisher, A. Tokay, J. Wang, and J. L. Pippitt, 2005: Ground validation for the Tropical Rainfall Measuring Mission (TRMM). *J. Atmos. Oceanic Technol.*, **22**, 365–379.
- Zrnica, D. S., and A. V. Ryzhkov, 1999: Polarimetry for weather surveillance radars. *Bull. Amer. Meteor. Soc.*, **80**, 389–406.
- , V. M. Melnikov, and J. K. Carter, 2006: Calibrating differential reflectivity on the WSR-88D. *J. Atmos. Oceanic Technol.*, **23**, 944–951.